Hindawi Publishing Corporation
Journal of Nanomaterials
Volume 2010, Article ID 710584, 11 pages
doi:10.1155/2010/710584

Research Article

Designated-Tailoring on {100} Facets of Cu_2O Nanostructures: From Octahedral to Its Different Truncated Forms

Zhimao Yang, Shaodong Sun, Chuncai Kong, Xiaoping Song, and Bingjun Ding

MOE Key Laboratory for Non-Equilibrium Synthesis and Modulation of Condensed Matter and State Key Laboratory for Mechanical Behavior of Materials, School of Science, Xi'an Jiaotong University, Xi'an, Shaanxi 710049, China

Correspondence should be addressed to Zhimao Yang, zmyang@mail.xjtu.edu.cn

Received 20 September 2010; Revised 10 November 2010; Accepted 16 November 2010

Academic Editor: Ali Eftekhari

A facile template-free controlled synthesis of Cu_2O architectures from octahedral to its different truncated forms is successfully achieved. It is found that the precursor formation temperature is crucial to the designated-tailoring on the {100} facets of Cu_2O crystals, which can modify the ratio (R) between the growth rates along the ⟨100⟩ and ⟨111⟩ directions, leading to the formation of the initial structures with different shapes. The multiple morphologies can be evolved from these varied initial structures via the synergic effect of oriented attachment and ripening mechanism. This template-free complex precursor-based solution route has provided an innovative approach to design the {100} facets with different sizes to further enrich the current morphologies of Cu_2O crystals.

1. Introduction

As a nonstoichiometric p-type semiconductor (direct band gap ~2.17 eV) with unique optical [1], magnetic [2], and negative expansion properties [3], Cu_2O (cuprous oxide) is a perspective material with applications in solar energy conversion [4], catalysis [5, 6], sensor [7, 8], negative electrode material for lithium-ion batteries [9], template [10, 11], metal-insulator-metal resistive switching memory [12], electrochromism [13, 14], and antibacterial activity [15]. To date, much attention has been devoted to the morphology-controlled synthesis of Cu_2O crystals, and Cu_2O crystals with different shapes have been fabricated, including cubes [16], octahedra [5], dodecahedra [17], 26-facets polyhedral [18, 19], nanowires [20], nanocages [21], multipods [22], hierarchical [7], and hollow structures [23]. Among these morphologies, highly symmetric structures (including cube, octahedron, and their truncated forms) are of particular interest due to their novel physical and chemical properties, which are different from other geometries by their intrinsic architectural characteristics with regard to lattice symmetry and surface energy [24]. Moreover, more complex structures can be derived from these simple structural forms [24], and their well-defined surfaces provide unique opportunities for the examination of their facet-specific properties [25]. However, the ability to elucidate the growth mechanism and shape-tailoring process of these polyhedral Cu_2O crystals is still limited.

Cu_2O has a cuprite structure with no free internal parameters. The structure is a cubic close packing of copper atoms, in which the coordination of the copper atoms is twice that of the oxygen atoms in a tetradecahedral unit cell [26–28]. A useful way that the anisotropic Cu_2O architectures could be formed in the solution condition is kinetically modifying the growth rates of different crystallographic planes of the Cu_2O by adopting appropriate reaction conditions [26, 29], which can lead to the variation of the ratio (R) between the growth rates along the ⟨100⟩ and ⟨111⟩ directions. Reference has demonstrated that the Wulff shape, such as an octahedron with four pairs of {111} facets or a cube with three pairs of {100} facets, can be easily formed [26]. However, the formation process of Cu_2O octahedra or cubes, and their truncated forms is primarily limited to additives-assisted solution synthesis. For example, Siegfried and Choi have fabricated cubes, octahedra, and their truncated forms via an additives-assisted electrochemical deposition

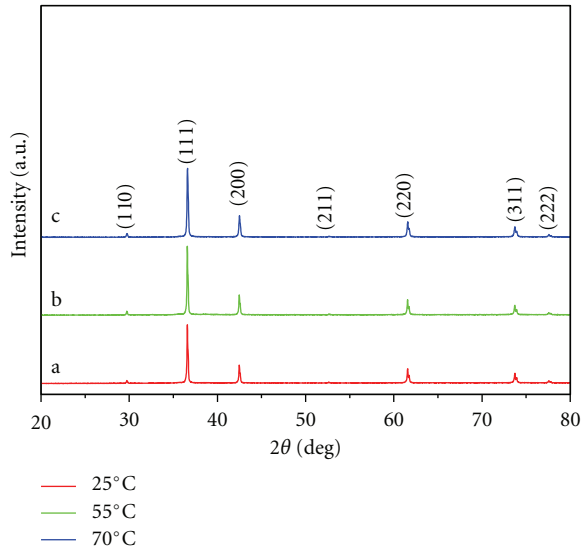

Figure 1: XRD patterns of (a) sample S1, (b) sample S2, and (c) sample S3.

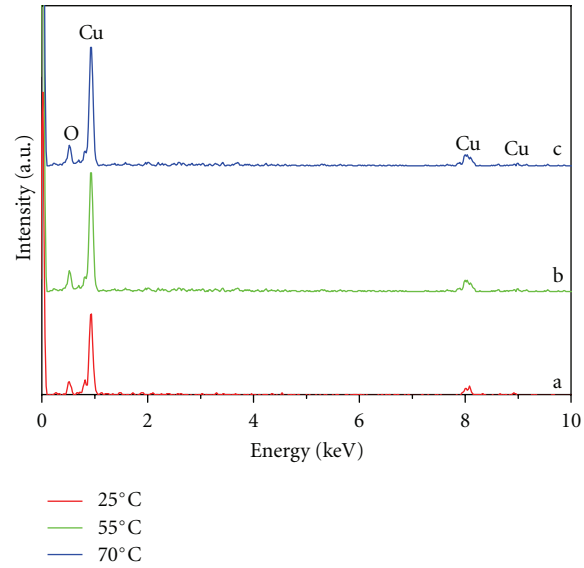

Figure 2: EDX spectra of (a) sample S1, (b) sample S2, and (c) sample S3.

[30, 31]. Kuo and Huang have reported Cu_2O Crystals with morphological evolution from cubic to octahedral structures by an SDS- (sodium dodecyl sulfate-) assisted solution synthesis [25]. Yang and Liu have achieved hexapod structures to octahedra and their truncated forms via a $Na_2(C_4H_4O_6)$ (sodium tartrate)-assisted hydrothermal route [32]. To our best knowledge, a template-free synthesis route for elucidating the shape evolution from octahedra to their different truncated forms was seldom reported, and it still remains a great challenge to systemically manipulate the sizes of truncated facets. Herein, we develop a facile and low-cost template-free complex-precursor aqueous solution synthesis method for designed-tailoring on {100} facets with different sizes to achieve the shape evolution of Cu_2O crystals from octahedral to its different truncated forms. The growth process and mechanism of Cu_2O crystals are discussed in detail.

2. Experimental Section

2.1. Preparation Procedures. All chemicals used in our experiment were of analytical grade and used without further purification. The synthetic procedure was described as follows: 0.825 g of $CuCl_2$ powder was dissolved in 50 mL deionized water using a beaker under a constant stirring at different temperature (25°C, sample S1; 55°C, sample S2; 70°C, sample S3). A precipitate was produced when a NaOH solution (3 M, 10 mL) was added dropwise to the above solution. In our paper, we describe the temperature of adding NaOH solution into the reaction system as the precursor formation temperature. After being stirred for 5 min, D-glucose powder (0.2 g) was added into the dark precursor with a constant stirring for 15 min at 70°C. The precipitate gradually turned brick red and then was allowed to cool to room temperature naturally. Afterward, the obtained particles were centrifuged at 5000 rpm for 1 min (XIANYI TG16-WS centrifuge). The precipitates were centrifuged twice more in deionized water and anhydrous ethanol, respectively and finally were dried at 70°C for 12 hours in a vacuum oven.

2.2. Characterization. The crystal phase of as-prepared products was characterized by an X-ray diffractometer (Bruker-AXS D8 ADVANCE) using Cu Kα radiation (λ = 1.54 Å) in the range (20° ~ 80°). The morphology of the powders was investigated by field emission scanning electron microscope (FESEM) using JEOL (JSM-7000F) at an accelerating voltage of 20 kV. EDX analysis was obtained with an Oxford INCA Energy dispersive X-ray detector installed on the JEOL JSM-7000F. The transmission electron microscopy (TEM) and high resolution transmission electron microscopy (HRTEM) analysis images were performed on a JEOL JEM-2100 transmission electron microscope operating at an accelerating voltage of 200 kV. Sample for the TEM analysis was prepared by ultrasonic dispersion for 30 s with ethanol (1.5 mL) in a 2 mL centrifuge tube. Then, the products were dropped onto a carbon-coated copper grid and dried in air before TEM analysis. The crystal structure of Cu_2O was drawn by using the Diamond 3.2 program. The ultraviolet-visible (UV-Vis) spectra were measured by a UV/vis/NIR spectrophotometer (Hitachi U-4100).

3. Results and Discussion

3.1. X-Ray Diffraction. The phase structure and purity of the products were examined by X-ray diffraction (XRD) characterization. Figure 1 shows the XRD patterns of the as-prepared products obtained at different precursor formation temperature (samples S1–S3). All the diffraction peaks of

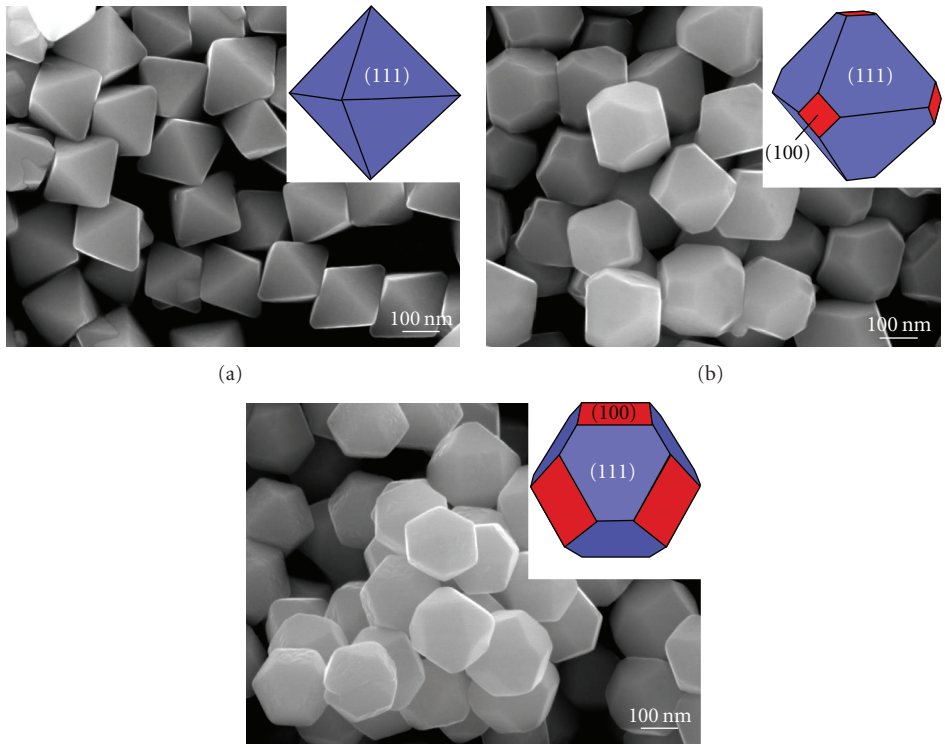

Figure 3: FESEM images of (a) sample S1, (b) sample S2, and (c) sample S3. The inserts are the corresponding schematic illustrations.

these three samples are indexed according to the standard cubic structure of Cu_2O (space group : $Pn\bar{3}m$, lattice constant $a = 0.427$ nm, JCPDS file no. 05-0667). No peaks of impurities such as copper or cupric oxide were detected, suggesting the high purity of the as-obtained products. Moreover, it is found that the ratio between the intensity of the (111) and (200) peak is higher than the standard value (3.25 versus 2.50 (sample S1), 3.06 versus 2.50 (sample S2), and 3.05 versus 2.50 (sample S3)). It is known that the facets with a slower growth rate will be exposed more on the crystal surface and exhibit relatively stronger diffraction intensity in the corresponding XRD pattern [33, 34]. Hence, it can be concluded that the products are abundant in {111} facets and the {100} facets might be exposed gradually in the final morphology due to the ratio between the intensity of the (111) and (200) peak decrease.

3.2. EDX Measurement. The chemical composition and purity of the products were examined by energy-dispersive X-ray spectroscopy. Figure 2 displays the electron energy dispersive X-ray (EDX) spectra of the as-prepared products obtained at different precursor formation temperature (samples S1–S3). It can be found that no peaks of impurities such as sodium and chlorine are detected, indicating the high purity of the as-obtained products. Only copper and oxygen are detected in the spectrum, and their atomic ratio is close to 2 : 1, confirming that the obtained products are Cu_2O crystals.

3.3. Morphological Observation. The morphology and size of the Cu_2O architectures were observed by field-emission scanning electron microscope. The precursor formation temperature was a crucial prerequisite for the formation of octahedral Cu_2O crystals with different truncated forms. Figure 3 shows representative FESEM images of the products obtained at different formation temperature of the cupreous complex precursor (samples S1–S3). From Figure 3(a), it can be seen that octahedral crystals are formed as the precursor formation temperature was 25°C (sample S1) and the octahedral Cu_2O crystals are about 600 nm in edges. Figure 3(b) is the FESEM image of the sample S2, which was obtained as the precursor formation temperature was 55°C. The products are truncated octahedral morphologies, and each particle has three pairs of squares and four pairs of hexagons. The edges of squares are about 220 nm in sizes, and the long edges of hexagon are about 450 nm. When the precursor formation temperature was increased to 70°C (sample S3), different truncated octahedra with larger square sections were synthesized. Figure 3(c) shows the typical FESEM image of sample S3. There are also two kinds of truncated sections, including squares and hexagons in these products, but the areas of the squares (440 nm × 440 nm) are larger than those of sample S2, while the sizes of the hexagons relatively decrease. The inserts as shown in Figures 3(a)–3(c) are schematic illustrations of the corresponding samples. According to Steno's law, the angles between two corresponding facets on the crystals are constant, thus the crystallographic planes can be well defined [35, 36]. Hence,

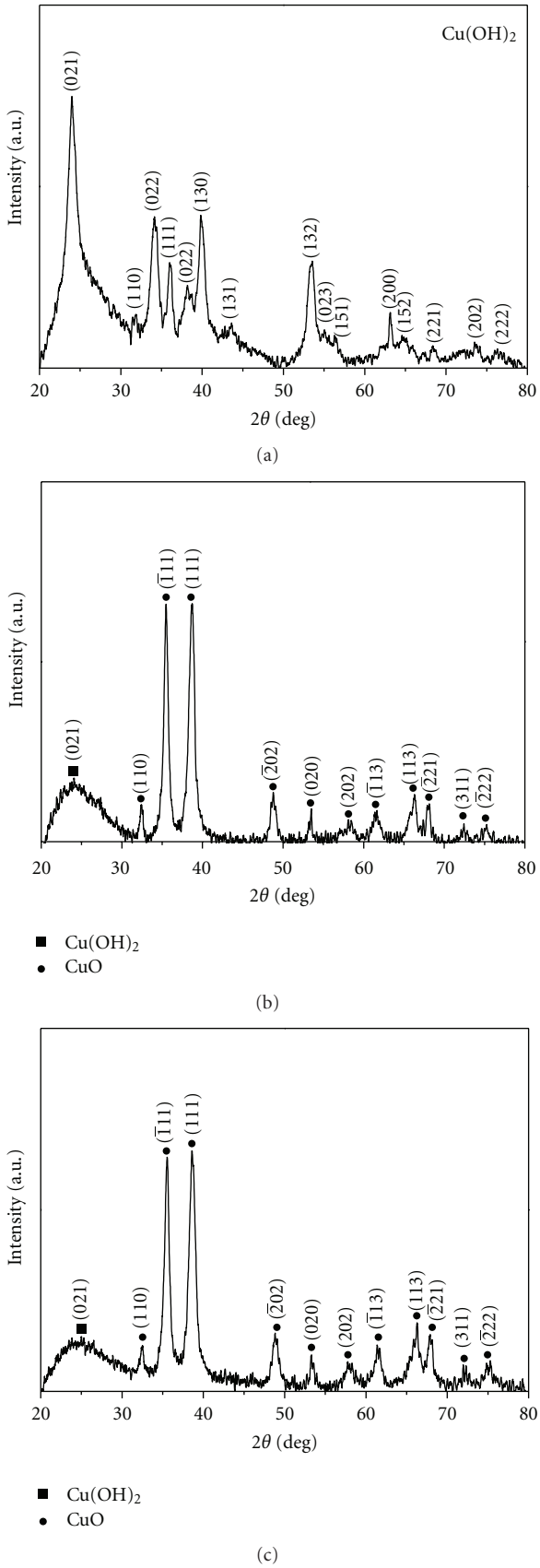

Figure 4: XRD patterns of the precursors obtained at different formation temperature ((a): 25°C; (b): 55°C; (c): 70°C).

the crystallographic planes denoted by blue color are similar to the {111} family, and the red areas (squares) are the {100} family. Based on the above analysis, it is believed that the shape evolution of Cu_2O crystals from octahedral to its different truncated forms can be achieved via controlling the precursor formation temperature.

3.4. Growth Mechanism. Our template-free complex precursor aqueous solution synthesis method is based on the reduction of $CuCl_2/NaOH/H_2O$ solution-phase system with D-glucose powder. The formation of Cu_2O crystals can be suggested as follows [37]:

$$Cu^{2+} + 2OH^- \longrightarrow Cu(OH)_2 \downarrow \quad (1)$$

$$Cu(OH)_2 + 2OH^- \longrightarrow [Cu(OH)4]2^- \quad (2)$$

$$2[Cu(OH)4]^{2-} + C_5H_{11}O_5\text{-}CHO \longrightarrow Cu_2O \downarrow + C_5H_{11}O_5\text{-}COOH + 4OH^- + 2H_2O \quad (3)$$

Cu^{2+} ions can coordinate with excess OH^- ions to generate $[Cu(OH)_4]^{2-}$complexes precursors [38]. Appropriate amount of D-glucose serves as a weak reducer at relatively high reaction temperature and can ensure the purity of products, which is in a manner similar to the reduction mechanism of reported D-glucose-based synthesis of Cu_2O crystals [17].

In this experiment, it has been found that the properties of complex precursors can be strongly affected by the precursor formation temperature. The XRD patterns of the precursors obtained at different formation temperature are shown in Figure 4. Figure 4(a) is the typical XRD pattern of the precursors obtained at the formation temperature of 25°C. It can be seen that all the diffraction peaks of the products are indexed according to the standard orthorhombic structure of $Cu(OH)_2$ (JCPDS file no. 80-0656), indicating that these precursors are pure $Cu(OH)_2$. The result is corresponding to the reaction mechanism. Figure 4(b) displays the XRD pattern of the precursors obtained at the formation temperature of 55°C. It is found that both the $Cu(OH)_2$ and CuO (JCPDS file no. 80-1268) are coexisted in the precursors. It is proposed that the $Cu(OH)_2$ were decomposed in higher reaction temperature, leading to the formation of CuO crystals. As the precursor formation temperature was increased to 70°C, the XRD pattern of the precursors (nanobelts) was given in the Figure 4(c), and it also has the diffraction peaks of both $Cu(OH)_2$ and CuO. Hence, the precursors prepared at different temperature have different phase structure, and it is proposed that the formation of Cu_2O architectures with different morphologies may be related to the characteristics of the complex precursors synthesized in different reaction conditions (1)–(3). The varied precursors formed in different temperatures can modify the reduction process (3), which might affect the competition between kinetics and thermodynamics during the reduction of precursors, nucleation, and growth of Cu_2O crystals.

Figure 5 is the typical TEM images of the precursors obtained at different formation temperature. Figures 5(a)

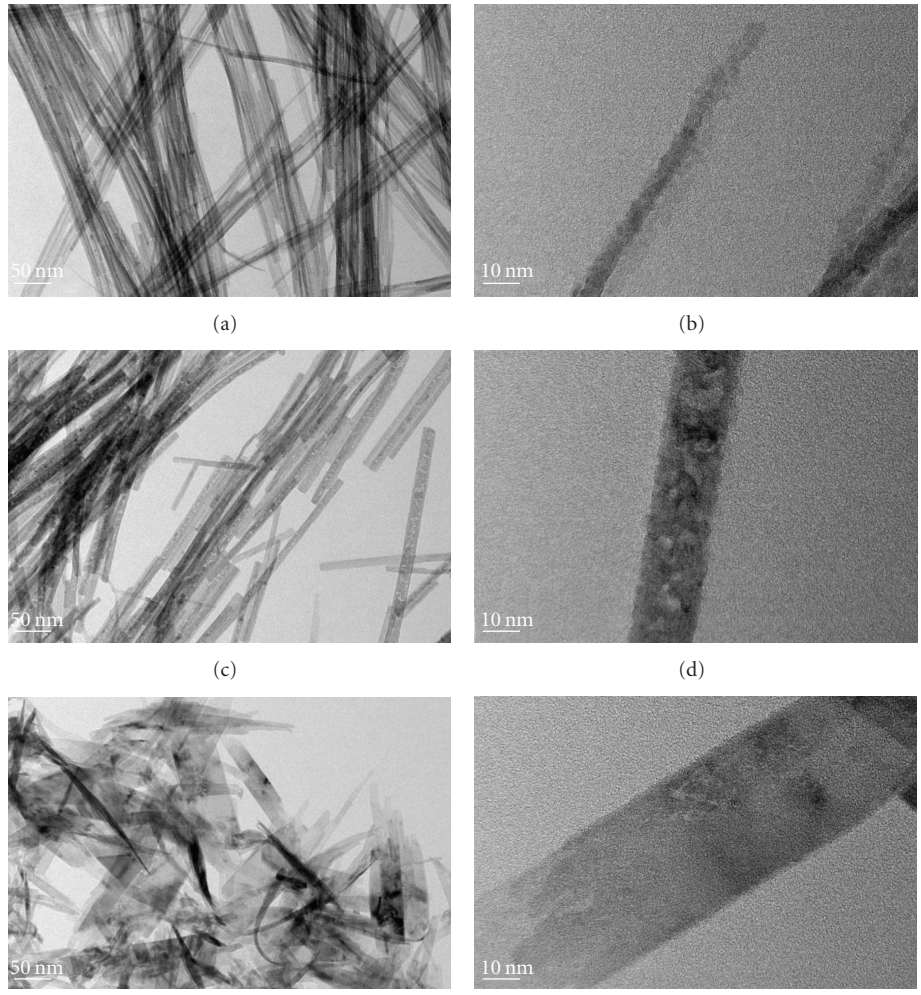

Figure 5: Low-magnification TEM images (a, c, e) and high-magnification TEM images (b, d, f) of the precursors obtained at different formation temperature ((a) and (b): 25°C; (c) and (d): 55°C; (e) and (f): 70°C).

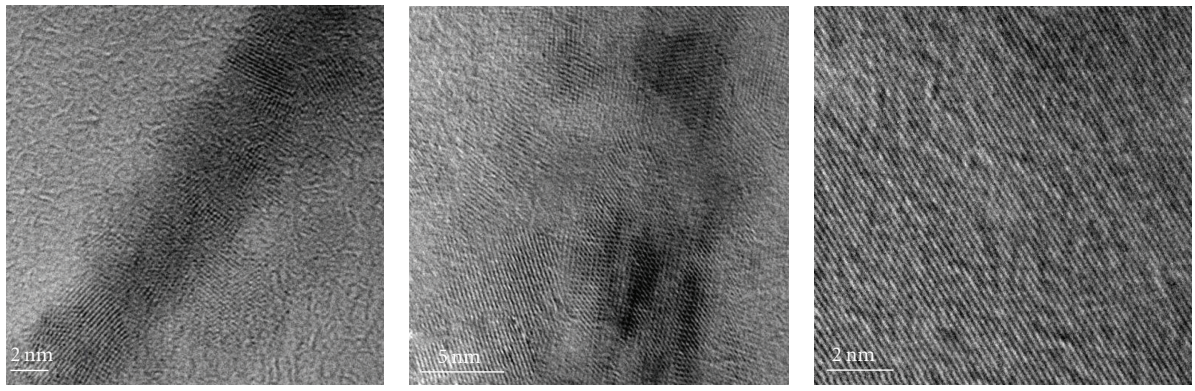

Figure 6: HRTEM images of the precursors obtained at different formation temperature ((a): 25°C; (b): 55°C; (c): 70°C).

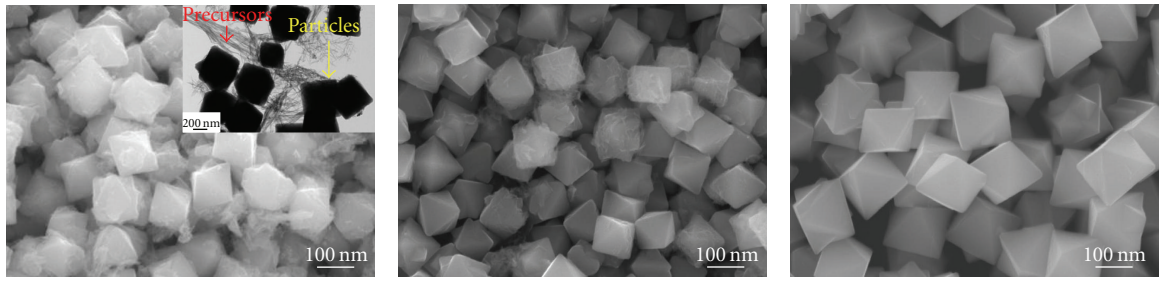

(a) (b) (c)

Figure 7: SEM images of the products obtained at different reaction temperature as the precursor formation temperature was 25°C ((a): 55°C, (b) 60°C, and (c) 68°C). The insert of (a) is the corresponding TEM images.

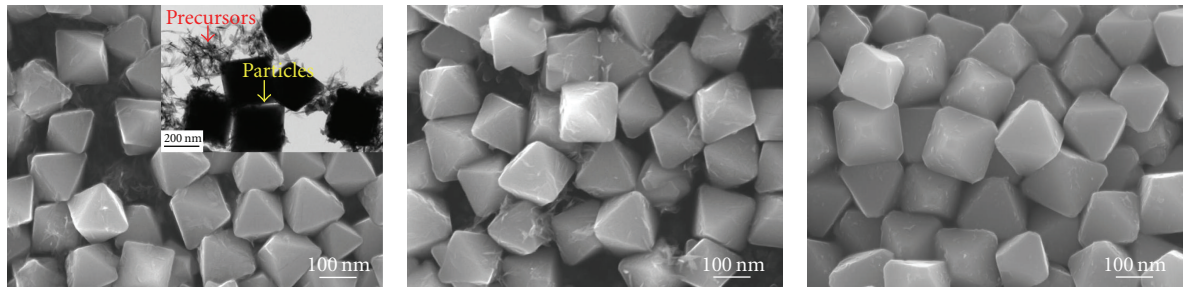

(a) (b) (c)

Figure 8: SEM images of the products obtained at different reaction temperature as the precursor formation temperature was 55°C ((a): 55°C; (b) 60°C; (c) 68°C). The insert of (a) is the corresponding TEM images.

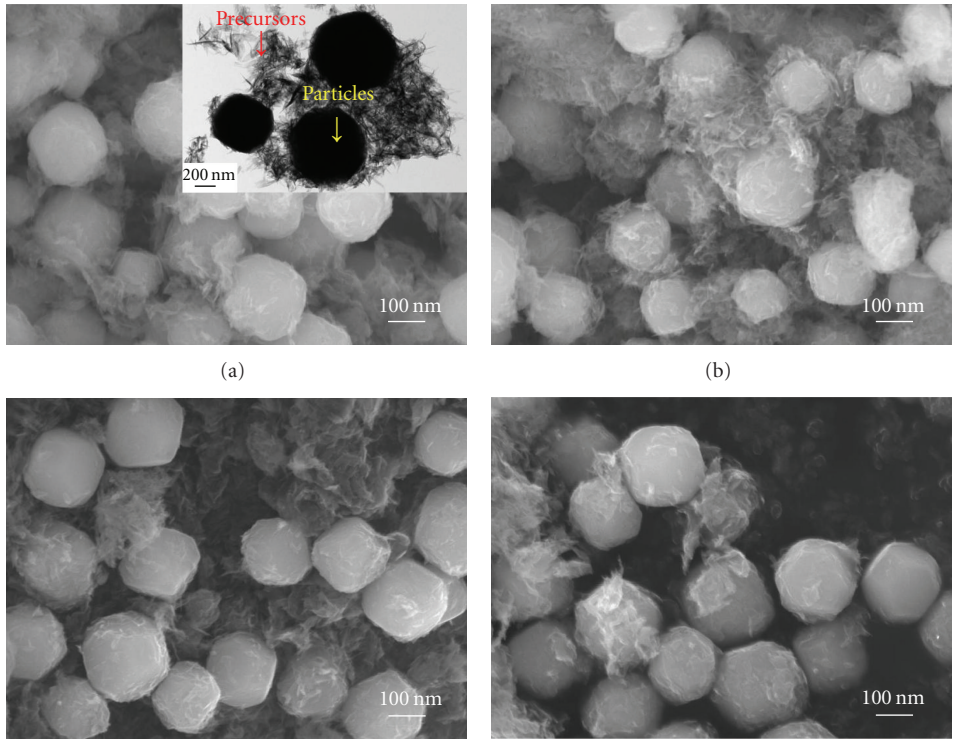

(a) (b)

(c) (d)

Figure 9: SEM images of the products obtained at different reaction time as the precursor formation temperature was 70°C ((a): 5 s, (b) 10 s, (c) 15 s, and (d) 30 s). The insert of (a) is the corresponding TEM images.

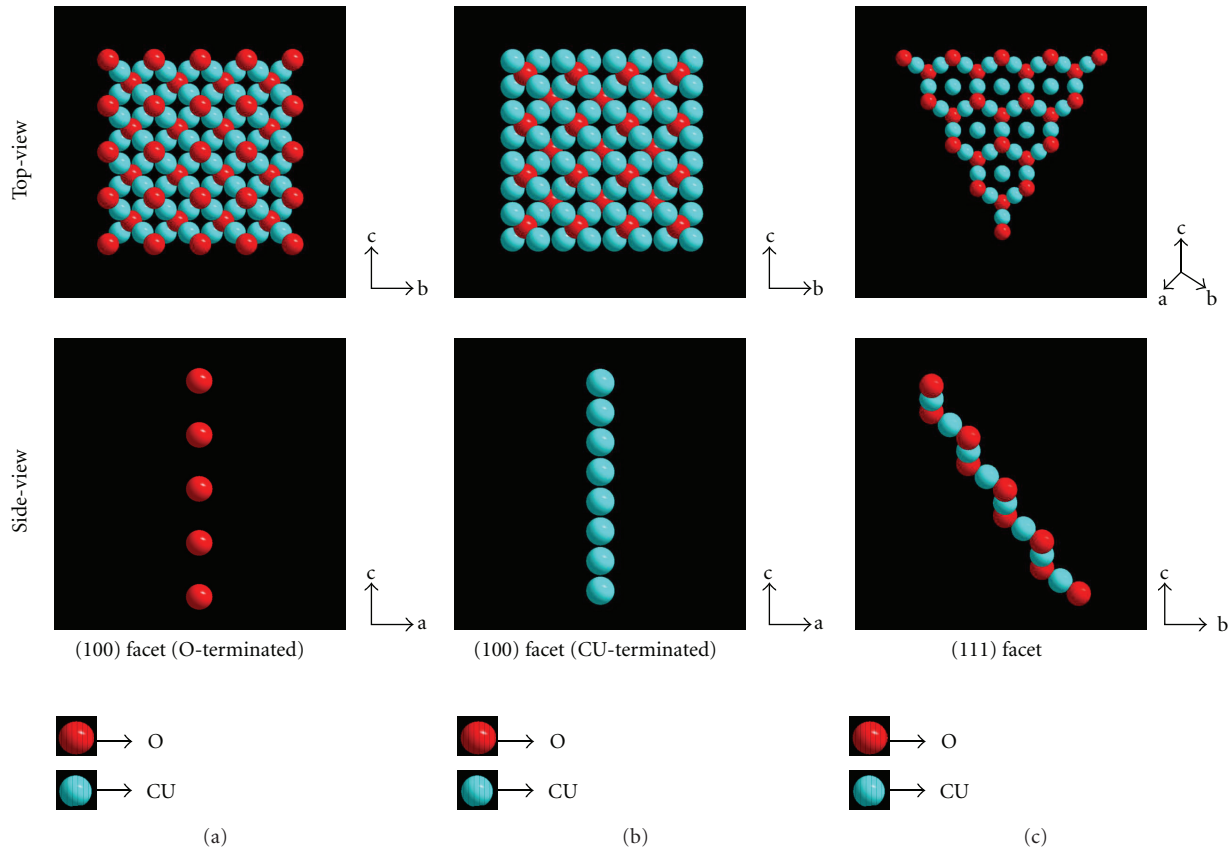

FIGURE 10: Crystallographic structures of (a) and (b) the (100), and (c) the (111) facets of Cu_2O.

and 5(b) are the low-magnification and high-magnification TEM images of the precursors prepared as the precursor formation temperature was 25°C. It can be found that the precursors are nanowires and the average diameter is about 8 nm. When the precursor formation temperature was 55°C, the precursors are still nanowires (Figures 5(c) and 5(d)), and the average length is less than that of Figure 5(a). The average diameter enhances up to about 25 nm. However, nanobelts are formed as the precursor formation temperature was 70°C, and Figures 5(e) and 5(f) are the low-magnification and high-magnification TEM images, respectively. The average length of the nanobelt is the shortest, but the width is about 50 nm. Figure 6 is the HRTEM images of the three precursors. It can be seen that the precursors synthesized at 25°C and 55°C are polycrystalline states (Figures 6(a) and 6(b)), while single crystal can be formed as the precursor formation temperature was 70°C (Figures 6(c)). Therefore, it is proposed that the formation of Cu_2O architectures with different morphologies may be related to the properties of complex precursors synthesized in different formation temperature.

To shed light on the formation mechanism of these Cu_2O crystals with different shapes (samples S1–S3), their growth process has been followed by examining the products obtained at different reaction stages. Figure 7 shows the FESEM images of the products obtained at different reaction temperature as the precursor formation temperature was 25°C. In this case, when the reaction temperature was 55°C, the FESEM images of products are shown in Figure 7(a), and the insert is the corresponding TEM image. It can be found that both octahedra particles and precursors (nanowires) are coexisted in this product. With the reaction temperature increased to 60°C, the amount of precursors was decreased (Figure 7(b)), and entire octahedra particles were formed as the reaction temperature was 68°C (Figure 7(c)). When the precursor formation temperature was 55°C, the intermediated products obtained at different reaction temperature are displayed in Figure 8. Figure 8(a) is the products obtained as the reaction temperature was 55°C, and the insert is the corresponding TEM image. It was observed that both octahedral and precursors (nanorods) were synthesized. However, truncated octahedral crystals were formed as the reaction temperature was 60°C (Figure 8(b)), and the precursors still adsorbed onto the truncated octahedral products, indicating that the reaction was not over at this time. When the reaction temperature was increased to 68°C, truncated octahedral Cu_2O crystals were entirely prepared (Figure 8(c)). Further enhancing the reaction time to 70°C for some minutes, the well-defined products can be synthesized (Figure 3(b)). When the precursor formation temperature was 70°C, the morphologies of intermediated products obtained at different reaction time (5 s, 10 s, 15 s, and 30 s) are shown in Figure 9. Figure 9(a) is the products obtained as the reaction time was 5 s, and the insert is the corresponding TEM image.

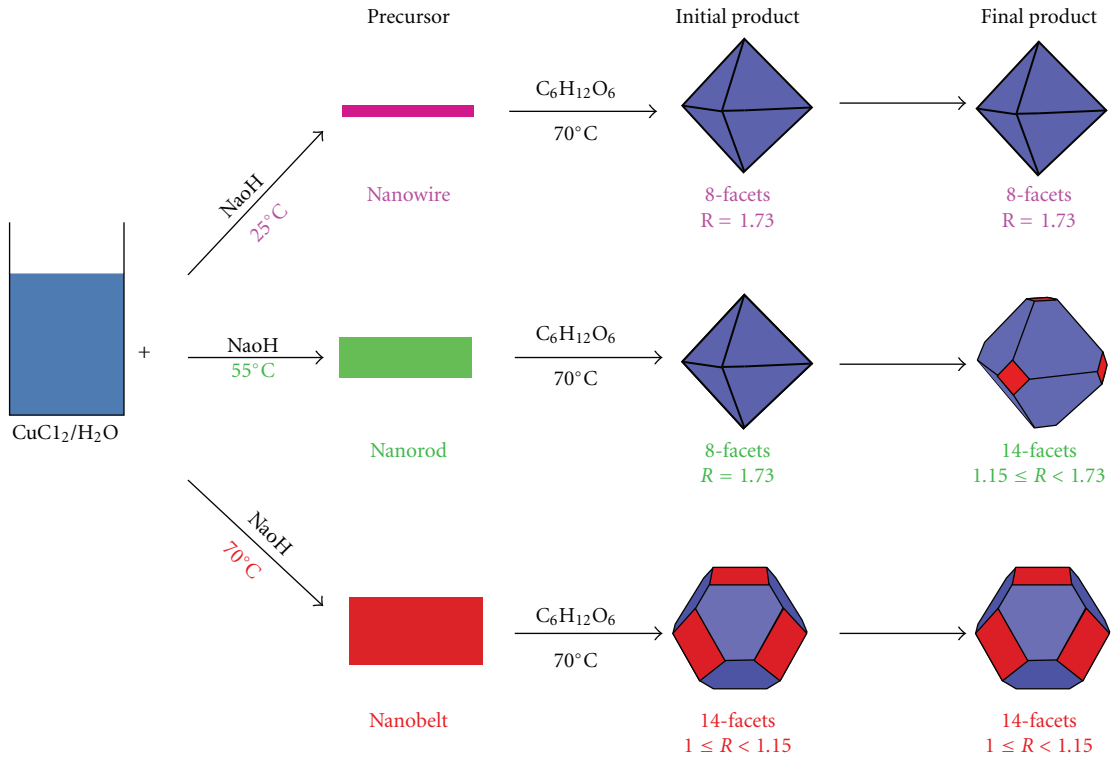

Figure 11: A schematic illustration of the proposed particle growth mechanism and reaction pathways that lead to the formation of Cu_2O crystals with different polyhedral shapes. As the essence of our synthesis, the precursors with different properties can be reduced by $C_6H_{12}O_6$ to form Cu_2O particles, which subsequently aggregate to form different initial structures. Subsequently, these initial structures will grow into various polyhedral forms through the synergic effect of oriented attachment and ripening mechanism, which can modify the ratio (R) between the growth rates along the ⟨100⟩ and ⟨111⟩ directions.

From the results, we can see that truncated octahedral Cu_2O crystals and nanobelts (precursors) were fabricated in the initial stage and the amount of nanobelts was decreased along with the reaction time increase (Figures 9(a)–9(d)), which suggests that the precursors were consumed continuously. Finally, truncated octahedra with larger {100} sections were formed (Figure 3(c)). Based on the above discussion, it is found that the polycrystalline precursors obtained at lower formation temperature (25°C and 55°C) can be reduced to octahedral structures in the initial stage, while single crystalline precursors prepared at higher formation temperature (70°C) are prone to generating 14-facet initial structures. Hence, the precursor formation temperature is a crucial parameter to determine the shape-evolution of Cu_2O architectures. However, the exact relation between precursors and shapes of Cu_2O crystals is worth further investigation.

In Cu_2O crystal lattice, due to the difference in electronegativities between Cu and O atoms, the {100} facets of Cu_2O are predominated by Cu or O atoms only (Figures 10(a) and 10(b)), leading to the electrically neutral state of {100} facets usually [39]. While the {111} facets are formed by both Cu and O atoms [26] and surface Cu atoms with dangling bonds on {111} facets can make them being positive charged (Figures 10(c)), {111} facets can be protected by negative charged molecules or ions [39]. The effect of anions used on the shape-controlled synthesis of crystals has been demonstrated [40], so it is believed that the presence of Cl^- ions can affect the shapes and sizes of the products in our experiment. It is proposed that the interaction strength between Cl^- ions and {111} facets might be not very strong at relatively lower reaction temperature, which results in the {111} facets (positive charged) to be easily protected by Cl^- ions (negative charged). An octahedral form enclosed with four pairs of triangle {111} facets (Figures 7(a) and 8(a)) was obtained when the R value between the growth rates along the ⟨100⟩ and ⟨111⟩ directions reached to 1.73 [25, 26, 41]. However, when the precursor formation temperature was higher (55°C), the surface energies of {111} facets could be to some extent enhanced along with the reaction temperature increase, thus the ratio R would be decreased ($1.15R < 1.73$), so the initial octahedral shape gradually evolved to its truncated forms (Figures 8(a) and 8(b)). The interaction strength between Cl^- ions and {111} facets might be further increased at higher reaction temperature (70°C) along with reaction time increase, leading to the surface energies of {111} facets further enhanced ($R \rightarrow 1.15$), thus the shapes as shown in Figure 3(b) were formed finally. For precursor formation temperature of 70°C, the interaction strength between Cl^- ions and {111} facets might be very strong, and the surface energies of {111} facets were enhanced, resulting in the increase of the growth rate along ⟨111⟩ directions. As the

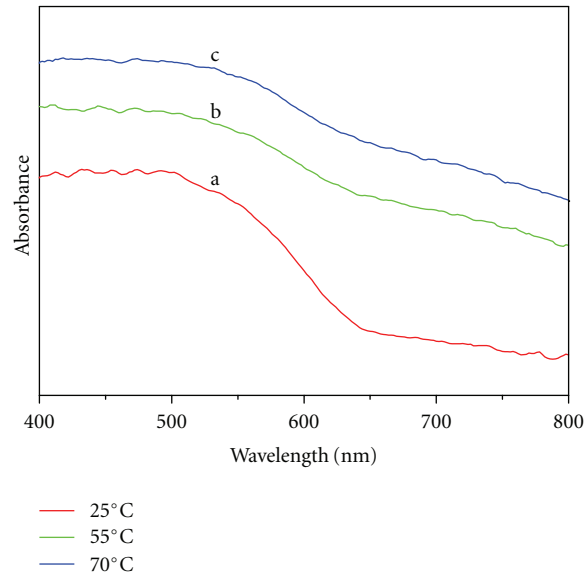

Figure 12: UV-vis spectra of (a) sample S1, (b) sample S2, and (c) sample S3.

ratio (R) between the growth rates along the ⟨100⟩ and ⟨111⟩ directions reached to 1.0 ~ 1.15 [25, 26, 41], a truncated octahedral shape (6 {100} and 8 {111} facets) was formed (Figure 3(c)). In our template-free complex-precursor-based solution route, a growth mechanism of these Cu_2O crystals is proposed. After addition of D-glucose powder into the reaction system, small Cu_2O seeds would be generated at relatively higher reaction temperature. In order to minimize the overall energy of the reaction system, seed particles tended to aggregate together (oriented attachment process), and the aggregates subsequently evolved into well-defined initial structures via a ripening mechanism [17, 38]. The initial structures with different shapes can be formed at different precursor formation temperature, which are shown in Figure 7(a), Figure 8(a), and Figure 9. In the present work, the morphology of these initial Cu_2O architectures is determined by the characteristic of precursors formed at different reaction temperature, which can modify the R values. As the reaction time increased, particles were continuously adsorbed onto these structures to allow further growth (ripening process) to generate Cu_2O crystals with different shapes. A schematic illustration of the proposed particle growth mechanism and reaction pathways is listed in Figure 11.

3.5. UV-Vis Measurement. Figure 12 shows the UV-vis spectra of Cu_2O products with different shape including octahedron (sample S1), truncated octahedron with different sizes of {100} facets (sample S2 and S3). The optical absorption edge of the octahedral Cu_2O crystals generates at about 643 nm, and we can calculate the band gap according to the absorption edge position [16], and the calculated band gap energy of sample S1 is about 1.93 eV. The optical absorption edge of the truncated octahedron with small section {100} facets (sample S2) occurs at about 630 nm, corresponding to the band gap energy of 1.97 eV. The optical absorption edge of the truncated octahedron with larger section {100} facets (sample S3) occurs at about 623 nm, corresponding to the band gap energy of 1.99 eV. All the band gaps are smaller than that those bulk Cu_2O (~ 2.17 eV).These absorption band positions are larger than those of the previousy reported nanocubes and nano-octahedra [25]. Moreover, the blue-shift (643 nm (sample S1) → 630 nm (sample S2) → 623 nm (sample S3)) has been observed along with the section areas of {100} facets increase.

4. Conclusions

Shape-controlled synthesis of Cu_2O architectures from octahedral to its different truncated forms is successfully achieved via a facile template-free aqueous synthesis route. It is found that the precursor formation temperature is crucial to designated-tailoring of the {100} facets of Cu_2O crystals, which can modify the ratio (R) between the growth rates along the ⟨100⟩ and ⟨111⟩ directions, leading to the formation of the initial structures with different shapes. The multiple morphologies can be evolved from these varied initial structures via the synergic effect of oriented attachment and ripening mechanism. Based on the relatively clear understanding of shape evolution and corresponding growth mechanism, this template-free complex precursor-based solution route has provided an innovative approach to design the {100} facets with different sizes to further enrich the current morphologies of Cu_2O crystals. Additionally, the UV-vis spectra suggest that the blue-shift has been observed along with the section areas of {100} facets increase.

Acknowledgments

The authors received financial support from the National Basic Research Program of China (no. 2010CB635101), National Science Foundation of China (NSFC nos. 51071116,

50871080, and 50901056), and National High Technology Research and Development Program of China (863 Program, no. 2009AA03Z320).

References

[1] Y. Tan, X. Xue, Q. Peng, H. Zhao, T. Wang, and Y. Li, "Controllable fabrication and electrical performance of single crystalline Cu_2O nanowires with high aspect ratios," *Nano Letters*, vol. 7, no. 12, pp. 3723–3728, 2007.

[2] A. Y. Yermakov, M. A. Uimin, A. A. Mysik et al., "Magnetism and structure of Cu_2O_{1+x} and 3d-doped TiO_{2-x} nanopowders," *Journal of Magnetism and Magnetic Materials*, vol. 310, no. 2, pp. 2102–2104, 2007.

[3] G. Artioli, M. Dapiaggi, P. Fornasini, A. Sanson, F. Rocca, and M. Merli, "Negative thermal expansion in cuprite-type compounds: a combined synchrotron XRPD, EXAFS, and computational study of Cu_2O and Ag_2O," *Journal of Physics and Chemistry of Solids*, vol. 67, no. 9-10, pp. 1918–1922, 2006.

[4] R. N. Briskman, "A study of electrodeposited cuprous oxide photovoltaic cells," *Solar Energy Materials and Solar Cells*, vol. 27, no. 4, pp. 361–368, 1992.

[5] H. Xu, W. Wang, and W. Zhu, "Shape evolution and size-controllable synthesis of Cu_2O octahedra and their morphology-dependent photocatalytic properties," *Journal of Physical Chemistry B*, vol. 110, no. 28, pp. 13829–13834, 2006.

[6] M. Hara, T. Kondo, M. Komoda et al., "Cu_2O as a photocatalyst for overall water splitting under visible light irradiation," *Chemical Communications*, no. 3, pp. 357–358, 1998.

[7] H. Zhang, Q. Zhu, Y. Zhang, Y. Wang, L. Zhao, and B. Yu, "One-pot synthesis and hierarchical assembly of hollow Cu_2O microspheres with nanocrystals-composed porous multishell and their gas-sensing properties," *Advanced Functional Materials*, vol. 17, no. 15, pp. 2766–2771, 2007.

[8] L. Guan, H. Pang, J. Wang, Q. Lu, J. Yin, and F. Gao, "Fabrication of novel comb-like Cu_2O nanorod-based structures through an interface etching method and their application as ethanol sensors," *Chemical Communications*, vol. 46, no. 37, pp. 7022–7024, 2010.

[9] P. Poizot, S. Laruelle, S. Grugeon, L. Dupont, and J. M. Tarascon, "Nano-sized transition-metal oxides as negative-electrode materials for lithium-ion batteries," *Nature*, vol. 407, no. 6803, pp. 496–499, 2000.

[10] S. Jiao, L. Xu, K. Jiang, and D. Xu, "Well-defined non-spherical copper sulfide mesocages with single-crystalline shells by shape-controlled Cu_2O crystal templating," *Advanced Materials*, vol. 18, no. 9, pp. 1174–1177, 2006.

[11] Z. Zhang, J. Sui, L. Zhang, M. Wan, Y. Wei, and L. Yu, "Synthesis of polyaniline with a hollow, octahedral morphology by using a cuprous oxide template," *Advanced Materials*, vol. 17, no. 23, pp. 2854–2857, 2005.

[12] A. Chen, S. Haddad, Y. C. Wu, T. N. Fang, S. Kaza, and Z. Lan, "Erasing characteristics of Cu_2O metal-insulator-metal resistive switching memory," *Applied Physics Letters*, vol. 92, no. 1, Article ID 013503, 2008.

[13] R. Neskovska, M. Ristova, J. Velevska, and M. Ristov, "Electrochromism of the electroless deposited cuprous oxide films," *Thin Solid Films*, vol. 515, no. 11, pp. 4717–4721, 2007.

[14] O. Akhavan, H. Tohidi, and A. Z. Moshfegh, "Synthesis and electrochromic study of sol-gel cuprous oxide nanoparticles accumulated on silica thin film," *Thin Solid Films*, vol. 517, no. 24, pp. 6700–6706, 2009.

[15] H. Pang, F. Gao, and Q. Lu, "Morphology effect on antibacterial activity of cuprous oxide," *Chemical Communications*, no. 9, pp. 1076–1078, 2009.

[16] HE. Y. Zhao, YE. F. Wang, and J. H. Zeng, "Hydrothermal synthesis of uniform cuprous oxide microcrystals with controlled morphology," *Crystal Growth and Design*, vol. 8, no. 10, pp. 3731–3734, 2008.

[17] X. Liang, L. Gao, S. Yang, and J. Sun, "Facile synthesis and shape evolution of single-crystal cuprous oxide," *Advanced Materials*, vol. 21, no. 20, pp. 2068–2071, 2009.

[18] H. Pang, F. Gao, and Q. Lu, "Glycine-assisted double-solvothermal approach for various cuprous oxide structures with good catalytic activities," *CrystEngComm*, vol. 12, no. 2, pp. 406–412, 2010.

[19] W. Zhou, B. Yan, C. Cheng et al., "Facile synthesis and shape evolution of highly symmetric 26-facet polyhedral microcrystals of Cu_2O," *CrystEngComm*, vol. 11, no. 11, pp. 2291–2296, 2009.

[20] Y. Xiong, Z. Li, R. Zhang, Y. Xie, J. Yang, and C. Wu, "From complex chains to 1D metal oxides: a novel strategy to Cu_2O nanowires," *Journal of Physical Chemistry B*, vol. 107, no. 16, pp. 3697–3702, 2003.

[21] C. Lu, L. Qi, J. Yang et al., "One-pot synthesis of octahedral Cu_2O nanocages via a catalytic solution route," *Advanced Materials*, vol. 17, no. 21, pp. 2562–2567, 2005.

[22] Y. Chang and H. C. Zeng, "Manipulative synthesis of multipod frameworks for self-organization and self-amplification of Cu_2O microcrystals," *Crystal Growth and Design*, vol. 4, no. 2, pp. 273–278, 2004.

[23] H. Zhang, X. Zhang, H. Li, Z. Qu, S. Fan, and M. Ji, "Hierarchical growth of Cu_2O double tower-tip-like nanostructures in water/oil microemulsion," *Crystal Growth and Design*, vol. 7, no. 4, pp. 820–824, 2007.

[24] J. Xu, S. Li, J. Weng et al., "Hydrothermal syntheses of gold nanocrystals: from icosahedral to its truncated form," *Advanced Functional Materials*, vol. 18, no. 2, pp. 277–284, 2008.

[25] C. H. Kuo and M. H. Huang, "Facile synthesis of Cu_2O nanocrystals with systematic shape evolution from cubic to octahedral structures," *Journal of Physical Chemistry C*, vol. 112, no. 47, pp. 18355–18360, 2008.

[26] J. Xu and D. Xue, "Five branching growth patterns in the cubic crystal system: a direct observation of cuprous oxide microcrystals," *Acta Materialia*, vol. 55, no. 7, pp. 2397–2406, 2007.

[27] J. M. Zuo, M. Kim, M. O'Keeffe, and J. C. H. Spence, "Direct observation of d-orbital holes and Cu-Cu bonding in Cu_2O," *Nature*, vol. 401, no. 6748, pp. 49–52, 1999.

[28] H. Raebiger, S. Lany, and A. Zunger, "Origins of the p-type nature and cation deficiency in Cu_2O and related materials," *Physical Review B*, vol. 76, no. 4, Article ID 045209, 2007.

[29] Y. Sui, W. Fu, H. Yang et al., "Low temperature synthesis of Cu_2O crystals: shape evolution and growth mechanism," *Crystal Growth and Design*, vol. 10, no. 1, pp. 99–108, 2010.

[30] M. J. Siegfried and K. S. Choi, "Elucidating the effect of additives on the growth and stability of Cu_2O surfaces via shape transformation of pre-grown crystals," *Journal of the American Chemical Society*, vol. 128, no. 32, pp. 10356–10357, 2006.

[31] S. Wu, Z. Yin, Q. He, X. Huang, X. Zhou, and H. Zhang, "Electrochemical deposition of semiconductor oxides on reduced graphene oxide-based flexible, transparent, and conductive electrodes," *Journal of Physical Chemistry C*, vol. 114, no. 27, pp. 11816–11821, 2010.

[32] H. Yang and Z. H. Liu, "Facile synthesis, shape evolution, and photocatalytic activity of truncated cuprous oxide octahedron microcrystals with hollows," *Crystal Growth and Design*, vol. 10, no. 5, pp. 2064–2067, 2010.

[33] Y. Sun and Y. Xia, "Shape-controlled synthesis of gold and silver nanoparticles," *Science*, vol. 298, no. 5601, pp. 2176–2179, 2002.

[34] O. Akhavan, "Silver nanocube crystals on titanium nitride buffer layer," *Journal of Physics D*, vol. 42, no. 10, Article ID 105305, 2009.

[35] H. G. Yang and H. C. Zeng, "Self-construction of hollow SnO_2 octahedra based on two-dimensional aggregation of nanocrystallites," *Angewandte Chemie International Edition*, vol. 43, no. 44, pp. 5930–5933, 2004.

[36] X. Zhao, Z. Bao, C. Sun, and D. Xue, "Polymorphology formation of Cu_2O: a microscopic understanding of single crystal growth from both thermodynamic and kinetic models," *Journal of Crystal Growth*, vol. 311, no. 3, pp. 711–715, 2009.

[37] S. Sun, F. Zhou, L. Wang, X. Song, and Z. Yang, "Template-free synthesis of weil-defined truncated edge polyhedral Cu_2O architectures," *Crystal Growth and Design*, vol. 10, no. 2, pp. 541–547, 2010.

[38] C. H. Kuo, C. H. Chen, and M. H. Huang, "Seed-mediated synthesis of monodispersed Cu_2O nanocubes with five different size ranges from 40 to 420 nm," *Advanced Functional Materials*, vol. 17, no. 18, pp. 3773–3780, 2007.

[39] J. Y. Ho and M. H. Huang, "Synthesis of submicrometer-sized Cu_2O crystals with morphological evolution from cubic to hexapod structures and their comparative photocatalytic activity," *Journal of Physical Chemistry C*, vol. 113, no. 32, pp. 14159–14164, 2009.

[40] M. Tsuji, K. Matsumoto, P. Jiang, R. Matsuo, X. L. Tang, and K. S. N. Kamarudin, "Roles of Pt seeds and chloride anions in the preparation of silver nanorods and nanowires by microwave-polyol method," *Colloids and Surfaces A*, vol. 316, no. 1–3, pp. 266–277, 2008.

[41] Z. L. Wang, "Transmission electron microscopy of shape-controlled nanocrystals and their assemblies," *Journal of Physical Chemistry B*, vol. 104, no. 6, pp. 1153–1175, 2000.